

pubs.acs.org/JPCA Article

Understanding Rapid PET Degradation via Reactive Molecular Dynamics Simulation and Kinetic Modeling

Shuangxiu Max Ma, Changlong Zou, Ting-Yeh Chen, Joel A. Paulson, Li-Chiang Lin,* and Bhavik R. Bakshi*



Cite This: J. Phys. Chem. A 2023, 127, 7323-7334



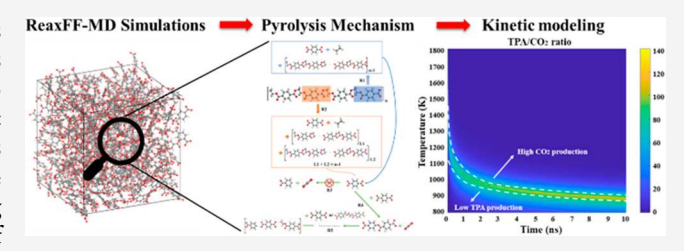
ACCESS I

III Metrics & More

Article Recommendations

s Supporting Information

ABSTRACT: As the demand for PET plastic products continues to grow, developing effective processes to reduce their pollution is of critical importance. Pyrolysis, a promising technology to produce lighter and recyclable components from wasted plastic products, has therefore received considerable attention. In this work, the rapid pyrolysis of PET was studied by using reactive molecular dynamics (MD) simulations. Mechanisms for yielding gas species were unraveled, which involve the generation of ethylene and TPA radicals from ester oxygen—alkyl carbon bond



dissociation and condensation reactions to consume TPA radicals with the products of long chains containing a phenyl benzoate structure and CO_2 . As atomistic simulations are typically conducted at the time scale of a few nanoseconds, a high temperature (i.e., >1000 K) is adopted for accelerated reaction events. To apply the results from MD simulations to practical pyrolysis processes, a kinetic model based on a set of ordinary differential equations was established, which is capable of describing the key products of PET pyrolysis as a function of time and temperature. It was further exploited to determine the optimal reaction conditions for low environmental impact. Overall, this study conducted a detailed mechanism study of PET pyrolysis and established an effective kinetic model for the main species. The approach presented herein to extract kinetic information such as detailed kinetic constants and activation energies from atomistic MD simulations can also be applied to related systems such as the pyrolysis of other polymers.

INTRODUCTION

With the increasing demand for plastic products in the packaging, film, construction, and electronics industries, developing strategies for converting plastic waste into valuable resources is critical.¹⁻³ Polyethylene terephthalate (PET) is a saturated polyester made from terephthalic acid (TPA) and ethylene glycol (EG), which is mainly used in light-plastic industries, such as water bottles, clothing accessories, and household items. However, landfills for PET should be limited due to the unsustainable environmental impact, as PET is difficult to degrade in the natural environment and continuously produces hazardous leachates and microplastics.² Instead of disposing of plastics in landfills, incineration is a widely used process to convert PET waste into heat resources; however, this process is associated with high carcinogenic potential emissions, such as heavy metals, dioxins, and nitrogen oxides. Although a relatively low environmental impact can be achieved with mechanical recycling, separating and cleaning PET waste is required. Also, the mechanical properties of recycled PET deteriorate significantly, leading to limited applications. Therefore, chemical recycling, such as pyrolysis and gasification, which converts plastic waste into hydrocarbon products, is a promising way to upgrade plastic waste. 5-7 It is more flexible than mechanical recycling and potentially less environmentally harmful than direct incineration.

Pyrolysis is a process that thermally decomposes plastic polymers, forming shortened intermediate species that can undergo further chemical reactions to produce a combination of smaller hydrocarbon molecules, liquids, and gases. The process is commonly classified by its temperature. Low-, medium-, and high-temperature pyrolysis are referred to as the temperature to be below 600 °C, 600–800 °C, and above 800 °C, respectively. Low-temperature treatments generally improve liquid products, while high-temperature operations enrich gaseous products. Both gaseous and liquid products are complicated combinations of hydrocarbons and other organic molecules whose composition depends on the nature of the plastic waste. 10,11

Numerous studies have been conducted to date to investigate pyrolysis processes involving PET plastic. For pure PET pyrolysis, Hrnjak-Murgic et al. 12 performed gas chromatography—mass spectrometry (GC-MS) analysis at low temperatures and proposed that the PET pyrolysis process can

Received: June 2, 2023 Revised: July 25, 2023 Published: August 24, 2023





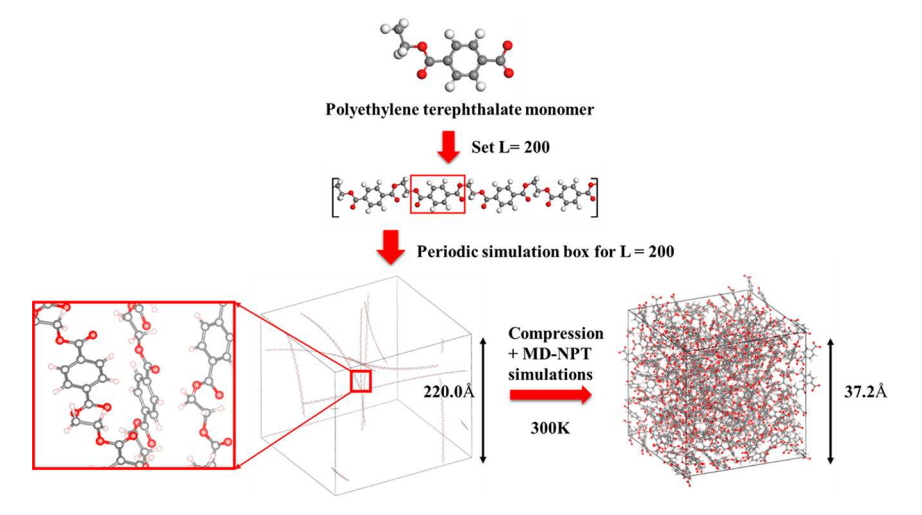


Figure 1. Illustration of the procedure to build the simulation system for PET pyrolysis: (1) Building a long PET chain (i.e., 200-monomer (L = 200), as shown) from a single monomer structure, and the molecule is placed in a large periodic domain. (2) The system was first compressed, followed by a simulation under the NPT ensemble to reach a reasonable density.

produce carbon dioxide, acetaldehyde, and benzoic acid. In addition, the authors showed that the concentration of the final products depends on the type of PET samples. Font et al. 13 determined the kinetic constants of the PET pyrolysis/ combustion hybrid process under a high-temperature oxygenrich environment. Pyrolysis-combustion mechanisms were proposed to explain the release of hazardous products such as ethylbenzene and naphthalene and highly toxic products such as phenol. As for PET copyrolysis, Pinto et al. 10,11 investigated the polyethylene-PET pyrolysis process under typical pyrolysis temperatures of 500-800 °C and detected end-product species. It was found that polyethylene increases the alkane content, while PET leads to a higher aromatic content in the product. In addition, extreme high-temperature copyrolysis was also used to produce high surface area carbon. 14,15 Aside from thermal degradation, it should be noted that catalytic cracking is also an effective means to modulate the final products through rational catalysis design. As a polyester with β -hydrogen, PET can be easily converted to aromatic hydrocarbons over catalysts possessing strong deoxygenation capabilities. ^{16–18} The addition of ZSM-5, ¹⁹ FeOOH, 20 and various metal oxides 21-23 has been demonstrated to inhibit the formation of terephthalic acid (TPA) and convert PET into aromatic-rich oils.

While significant progress has been made in studying the decomposition of PET, molecular-level observations of PET pyrolysis and detailed reaction models capable of describing the process remain missing. Theoretical simulations reported to date either focused on employing quantum chemistry to study a small PET dimer system²⁴ for some local chemical properties of pyrolysis cracking or using kinetic-based approaches²⁵ to describe plastic pyrolysis and predict gas, liquid, and residual solid species. The former may not capture the complete reaction pathway, while the latter cannot describe the time-dependent evolution of the chain length and product distribution at the molecular level. To address these challenges, molecular dynamics (MD) simulations using reactive force fields (i.e., denoted as ReaxFF MD hereafter) coupled with developing a detailed kinetic model to describe the main species observed in the atomistic simulations may represent a powerful approach. Reactive force fields are bond-order-based potentials developed by van Duin et al.,²⁶ which can describe

the association and disassociation of bonds. This enables the simulations of large systems involving chemical reactions with high accuracy.²⁷ In recent years, ReaxFF MD simulations have been widely used to simulate various systems, such as the thermal decomposition and catalytic cracking of hexadecane by Sun et al., 28,29 complex combustion processes by Zhang et al.,30 the incomplete combustion mechanism of multicomponent fuel by Zhao et al.,³¹ and the copyrolysis of coal and polyethylene/polystyrene by Guo et al. 32 However, ReaxFF MD simulations are typically performed under temperatures much higher than the experimental conditions to accelerate the observation of reaction events. To this end, establishing a rational workflow is crucially needed to develop a kinetic model based on the data from molecular simulations that extends the results of atomic-level observations to practical conditions

In this study, ReaxFF MD simulations were carried out to study the pyrolysis of PET at the atomic level and shed light on its reaction mechanism. Moreover, based on the obtained MD trajectories, a kinetic model was developed for describing the evolution of main species over time, and the model was exploited to identify optimal reaction conditions.

COMPUTATIONAL DETAILS

Molecular Dynamics (MD) Simulations and PET Models. Molecular dynamics (MD) simulations were performed to study PET pyrolysis. A long-chain PET polymer was constructed using the Moltemplate package³³ and placed in a periodic simulation box to mimic the structural characteristics of long-chain polymers that extend in all directions. PET polymers of different monomer numbers (i.e., L = 100, 200, and 400, corresponding to the molecular weight of 19,200-76,800 g/mol) were constructed to cover the typical molecular weight of PET polymer for simulation 34,35 and investigate the influence of the chain length. Figure 1 depicts the PET model studied in this work. The box initially had a large dimension of $220 \times 220 \times 220 \text{ A}^3$ to avoid chain overlaps. To achieve a more reasonable starting point, nonreactive force fields were first adopted to compress the domain. Specifically, the optimized potentials for liquid simulations for all atoms (OPLS-AA) force field were applied, and the sparse system was first compressed to $30 \times 30 \times 30 \times 30$ Å³

with a change rate of 0.019 Å /ps in the box dimension. The ReaxFF was then applied to further refine the initial structure in the isothermal-isobaric ensemble (i.e., NPT ensemble with pressure = 1 atm and temperature = 300 K) to relax the structure. The average density observed during the NPT simulation was 1.34 g/cm³, which is in excellent agreement with the experimentally reported density ranging from 1.33 to 1.40 g/cm^{3.35} More discussion on the adopted ReaxFF force field and its validation will be given in later sections. The ReaxFF-MD simulations were then performed under the canonical ensemble (i.e., NVT ensemble) with a Nosé-Hoover thermostat to simulate PET pyrolysis. The temperature of the systems was first ramped up to the desired temperature at a heating rate of 100 K/ps, followed by holding at the target temperature for one ns. A time step of 0.1 fs and a temperature damping constant of 100 fs were used in all of the ReaxFF MD simulations. For better statistics, five independent ReaxFF MD calculations with different random seeds were performed for each condition. Results presented were the averages of the observations made in those five simulations. Table S1 of the Supporting Information (SI) summarizes the PET systems (i.e., varying lengths and temperatures) studied in this work. All the MD simulations were performed using the open-source LAMMPS code.³⁶ Simulation input files for reactive MD simulations can be found in the SI.

Reactive Force Field. Molecular simulations require reliable descriptions of inter- and intramolecular interactions. Ideally, quantum mechanical (QM) methods may be employed to capture such interaction energies at a high accuracy if their computational cost is not prohibitively large. To this end, a set of parameters with given mathematical expressions is adopted for this purpose, which is termed the force field. While traditional force fields were not designed to simulate bond association and dissociation, reactive force fields (ReaxFF)²⁶ were proposed. Such force fields are based on the so-called bond orders determined by the distance between pairs of atoms. Various energy contributions can then be accordingly computed, including bond energy (E_{bond}) , overcoordination energy (E_{over}) , undercoordination energy (E_{under}) , valence angle energy $(E_{\rm val})$, penalty energy $(E_{\rm pen})$, torsion energy $(E_{\rm tors})$, conjugation energy $(E_{\rm conj})$, and nonbond van der Waals (E_{vdWaals}) and Coulomb (E_{Coulomb}) interactions. Owing to the complexity of the force field, it contains tens or even hundreds of parameters typically trained against highly accurate density functional theory (DFT) calculations.²⁶ In this work, the reactive force field developed by van Duin et al.²⁷ for the oxidation of hydrocarbons was used to describe the PET pyrolysis process; this force field has also been successfully utilized in MD studies for various systems involving oxygencontaining long-chain reactants and proved to be able to capture their reactive behavior as reported in numerous studies. 28,29,32,37,38

Kinetic Models. Kinetic models containing a set of ordinary differential equations (ODEs) to describe various key reactions observed in pyrolysis simulations were developed according to the main reaction routes observed from the MD simulations. These reactions were all considered first-order. In this study, the ODE system was solved by using the fourth-order Runge–Kutta method (ode45). The nonlinear optimization solver (i.e., lsqnonlin) implemented in MATLAB was also used to optimize the coefficients involved in the model (i.e., rate and activation constants) by minimizing the mean square error (RMSE) between the number of molecules

determined using the model and that observed from MD simulations.

RESULTS AND DISCUSSION

In this section, the accuracy of the force field was first validated. Commonly observed species and changes in the chain length were then discussed to give an atomistic overview of the PET pyrolysis, followed by discussions on the effects of temperature and chain length, as well as the reaction pathways. Subsequently, this section discusses the development of kinetic models capable of bridging the results of atomistic simulations and practical pyrolysis processes of a greater time scale and lower temperature, followed by analyses to explore the optimal reaction condition.

Force Field Validation. Aside from the agreement between the simulated density and that measured experimentally, as noted above, the activation energies of PET pyrolysis were computed by MD simulations and compared with experimental results to further validate the adopted potential. Specifically, in these calculations, the PET system was heated from 1600 to 2000 K at a rate of 100 K/ps. The logarithm of the reaction rate constants calculated from the mass loss ratio (i.e., $(m_{\text{total}} - m_{\text{solid}})/m_{\text{total}}$) is plotted versus the reciprocal temperature (1/T), as shown in Figure 2. The

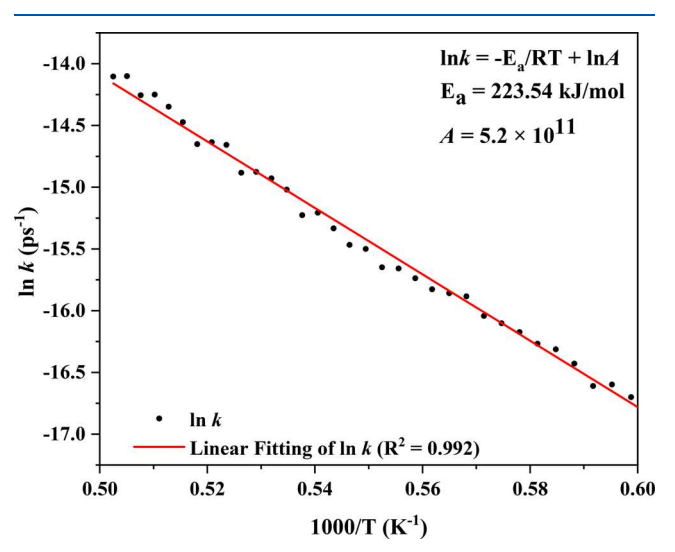


Figure 2. Determination of the activation energy $(E_{\rm a})$ and pre-exponential factor (A), per the Arrhenius form, for PET pyrolysis. The logarithm of reaction rate constants calculated from the MD-computed mass loss ratio (i.e., $(m_{\rm total}-m_{\rm solid})/m_{\rm total})$ is plotted vs 1000/T (T stands for temperature).

activation energy $(E_{\rm a})$ and pre-exponential factor (A) were accordingly determined to be 223.54 \pm 3.34 kJ/mol and 5.2 \times 10¹¹, respectively. The $E_{\rm a}$ obtained in this work resembles the experimental data ranging from 192.0 to 230.7 kJ/mol (see details in Figure S1 and Table S3 with further discussion). The results shown here further confirm the suitability of the adopted force field to study the PET system, particularly its reaction properties.

Chain Breaking and Main Species. The changes in the PET chain length were first analyzed to understand the chain-breaking process in pyrolysis. Figure 3a shows that the chain cracking at an elevated temperature is a fast process with the release of small molecules; at the temperature of 1600 K, the number of carbon atoms in the longest chain reduced rapidly,

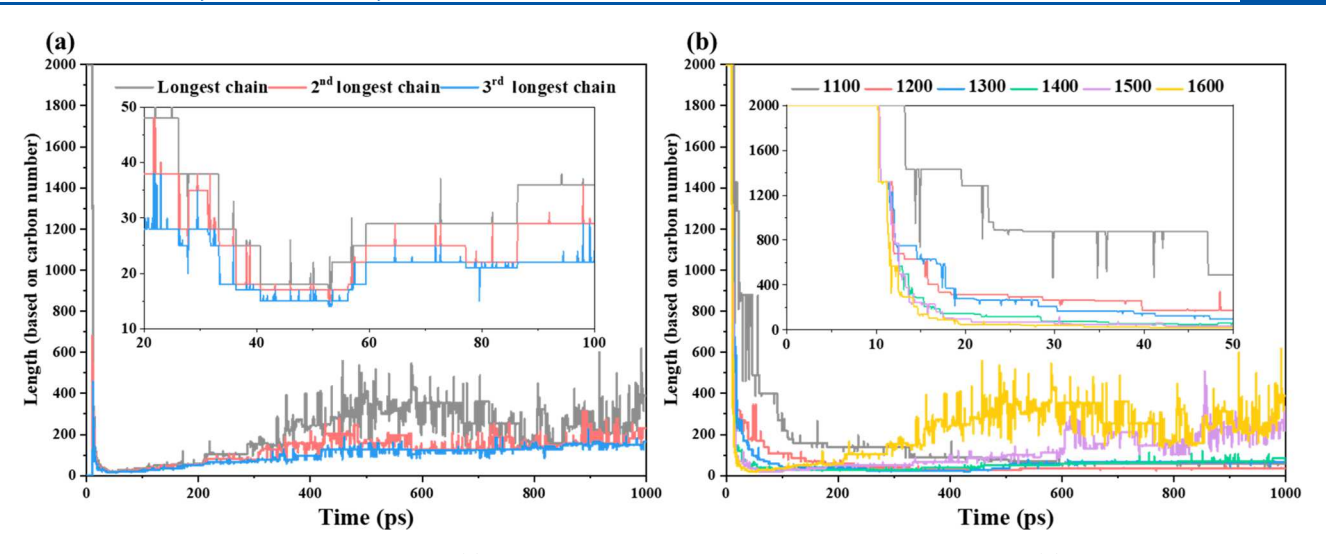


Figure 3. Time evolution of the carbon number of (a) 1st, 2nd, and 3rd longest chain species observed at 1600 K. (b) Length change of the longest chain at temperatures ranging from 1100 to 1600 K. The insets show the simulation observations at the initial stage (i.e., 20–100 and 0–50 ps for (a) and (b), respectively).

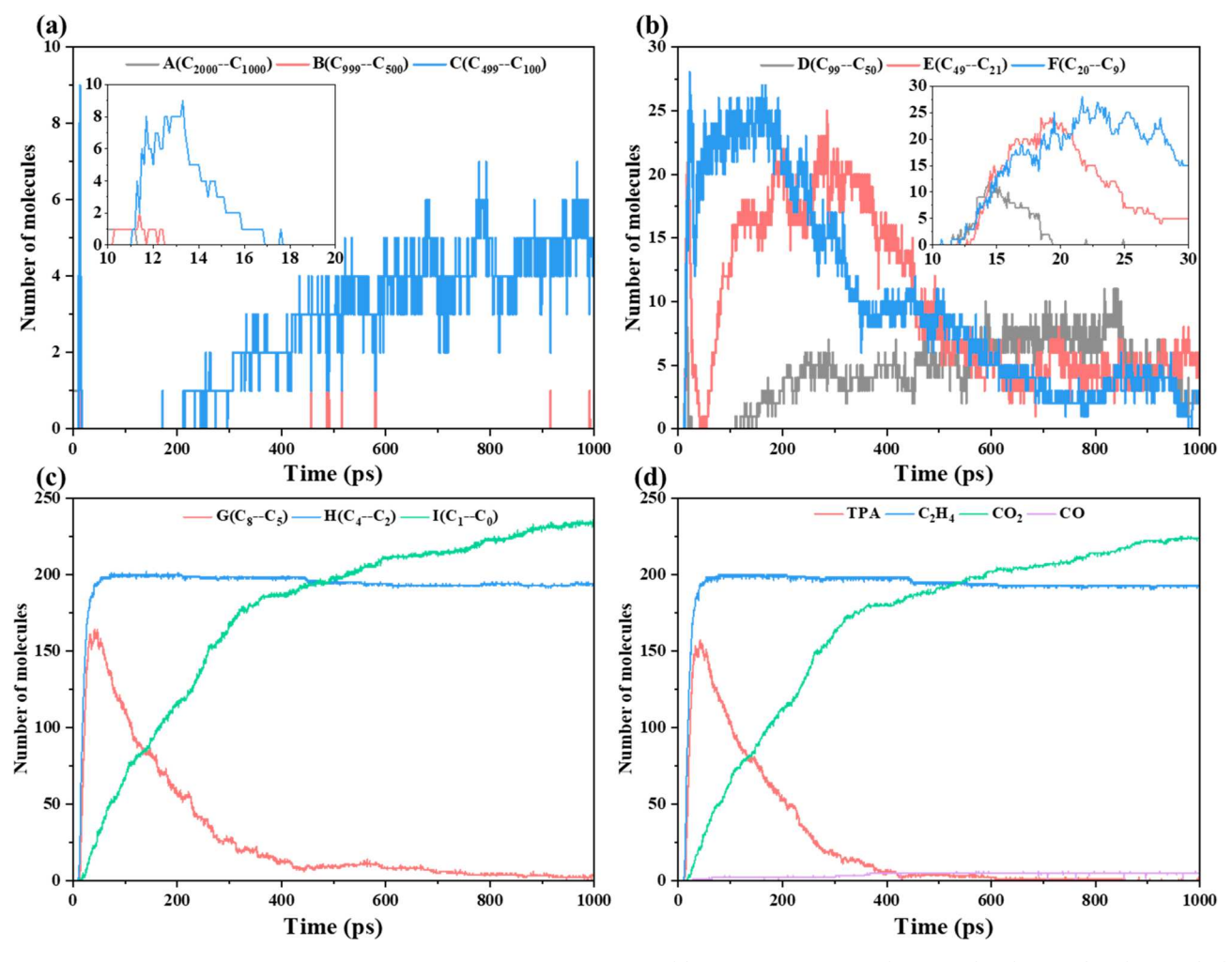


Figure 4. Time evolution of species classified with carbon numbers at 1600 K: (a) long-chain species: $A(C_{2000-1000})$, $B(C_{999-500})$, $C(C_{499-100})$, (b) midchain species: $D(C_{99-50})$, $E(C_{49-21})$, $E(C_{20-9})$, and (c) short-chain species: $D(C_{8-5})$, $D(C_{4-2})$, $D(C_{1-0})$, and (d) are commonly observed species during the simulation.

and from the subplot of Figure 3a it is noted that the longest chain length was less than 40 from an initial long chain with 2000 carbon atoms within 40 ps, and the chain length will

increase after it reached the minimum point. Snapshots of the simulated system can also be seen in Figure S2. Interestingly, as the reaction proceeded, the carbon number of the longest

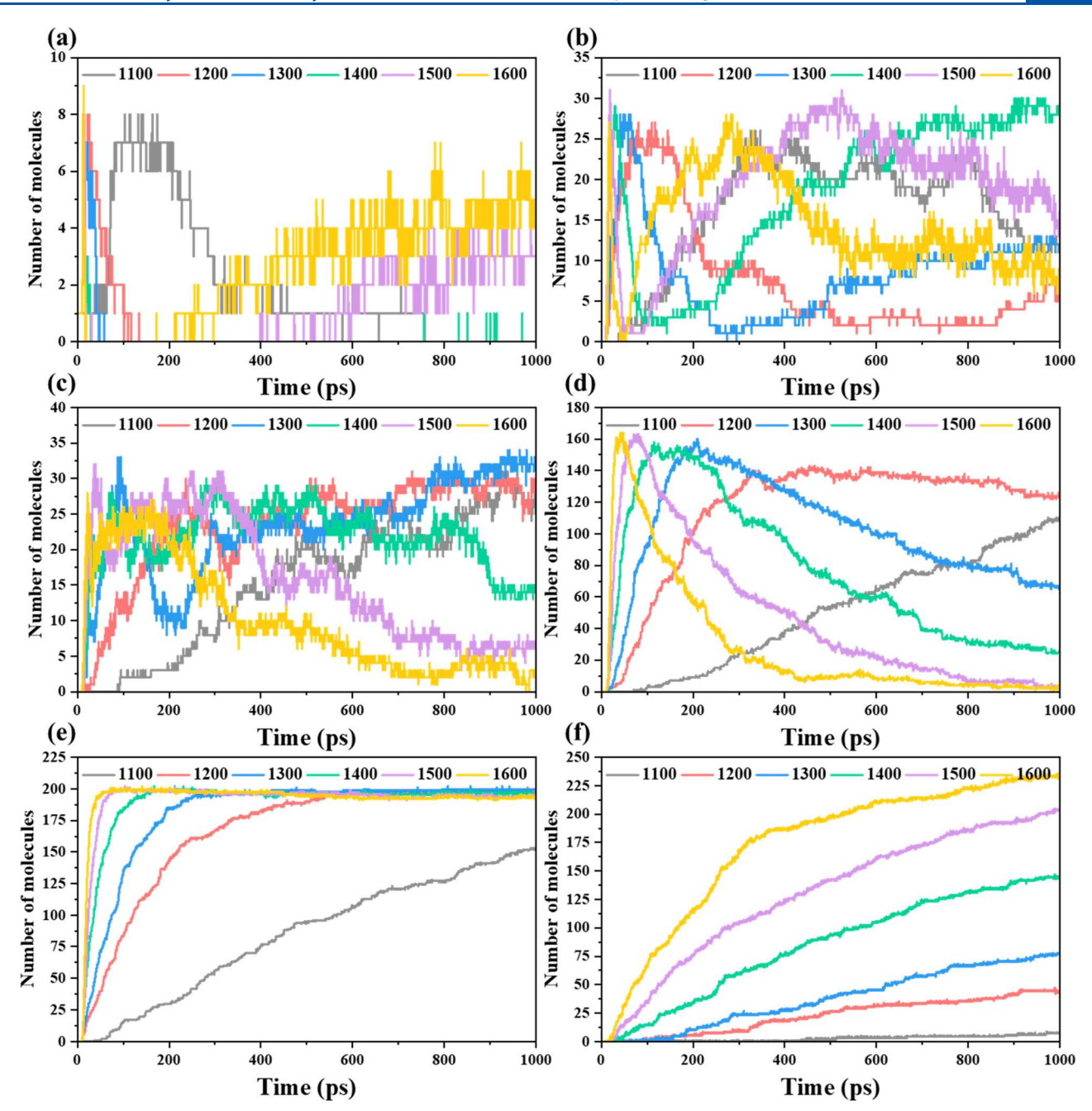


Figure 5. Time evolution of (a) long-chain, (b) midchain, (c) $C_{20}-C_9$, (d) C_8-C_5 (primarily TPA radical), (e) C_4-C_2 (primarily C_2H_4), and (f) C_1-C_0 (primarily CO_2) species at temperatures ranging from 1100 to 1600 K.

chain was found to increase counterintuitively. Since if there only existed chain breaking reactions, only the decrease in chain length would be observed. This phenomenon indicates that short-chain species can merge into longer-chain species. Figure 3b compares the length changes of the longest chains observed at different temperatures. A trend of rapid decrease was observed at the beginning stage (see the subplot of Figure 3b), and the increase of the chain length in a later stage is more prominent at higher temperatures. To understand the release of small gas molecules and such long-chain reforming, the evolution of species observed during the simulation was extracted with the main species identified. For clarity and simplicity, all species observed in simulations were classified into nine categories according to their chain length: $A(C_{2000-1000})$, $B(C_{999-500})$, $C(C_{499-100})$, $D(C_{99-50})$, $E(C_{49-21})$,

 $F(C_{20-9})$, $G(C_{8-5})$, $H(C_{4-2})$, and $I(C_{1-0})$, where C_{n-m} represents the range in the number of carbon atoms. For species $C(C_{499-100})$, $D(C_{99-50})$, $E(C_{49-21})$, and $F(C_{20-9})$, Figure 4a,b shows that distinct peaks were observed for these long/midchain species: the first peak (observed in the early stage of the reaction, see insets) represents the breaking process from longer chains into shorter chains. For example, the first peak of $C_{499-100}$ was formed by the decomposition of $C_{999-500}$ into $C_{499-100}$ and the decomposition of $C_{499-100}$ itself. The second peak indicates that these short-chain species can reform into long-chain species after the cracking of the longer chains. Meanwhile, Figure 4c demonstrates that $G(C_{8-5})$, $H(C_{4-2})$, and $I(C_{1-0})$ are the most prominent species whose number increased sharply to a relatively high value compared to other species with a longer chain length. By comparison of

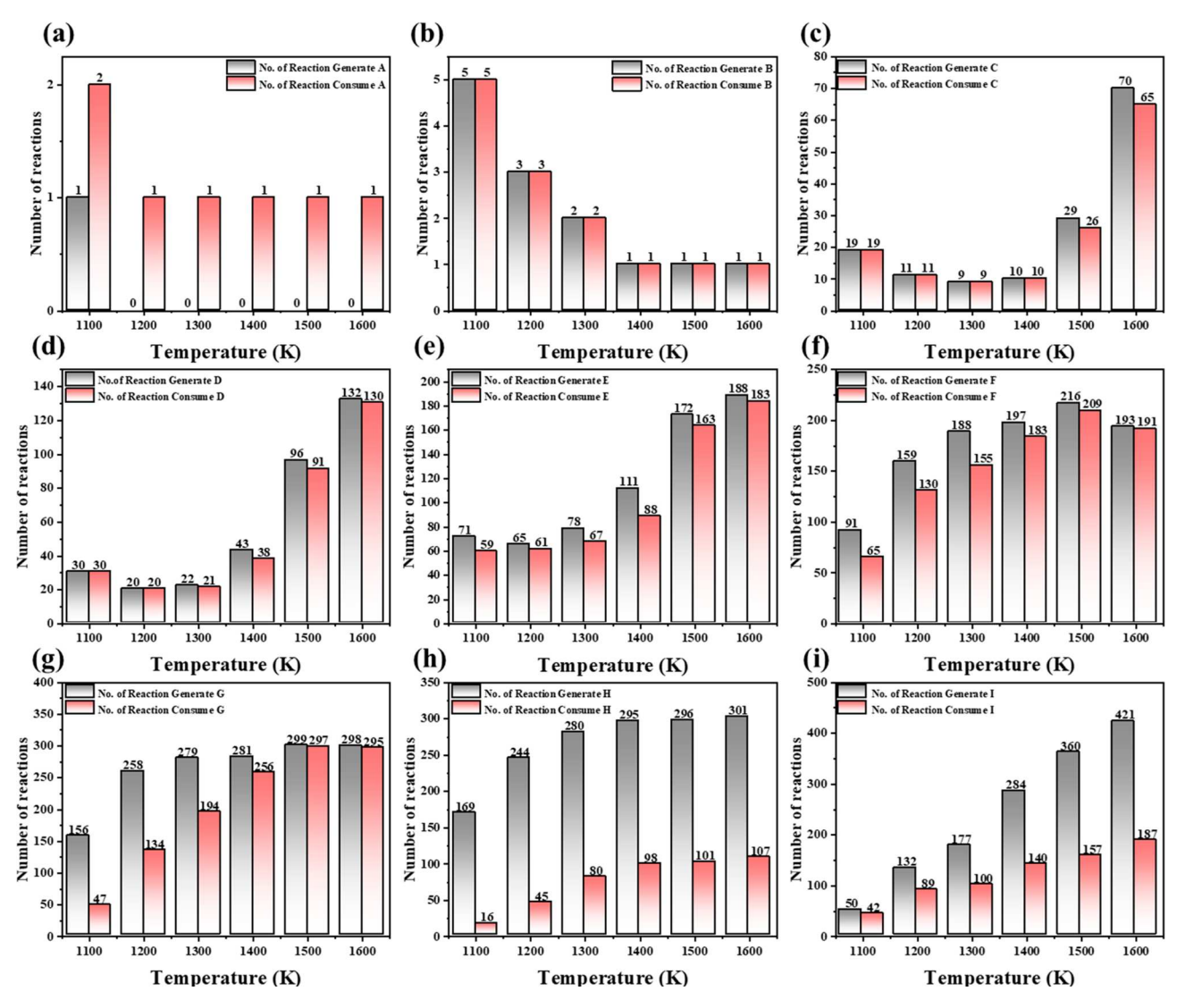


Figure 6. Total number of generation and consumption reaction events observed during simulations of 1 ns at temperatures ranging from 1100 to 1600 K. For clarity, species are classified by their length into nine groups: $A(C_{2000-1000})$, $B(C_{999-500})$, $C(C_{499-100})$, $D(C_{99-50})$, $E(C_{49-21})$, $F(C_{20-9})$, $G(C_{8-5})$, $H(C_{4-2})$, and $I(C_{1-0})$.

the results shown in Figure 4d, it is found that the main components of $G(C_{8-5})$, $H(C_{4-2})$, and $I(C_{1-0})$ are TPA, C₂H₄, and CO₂, respectively. During the pyrolysis, ethylene molecules were first formed, with the number increasing sharply and peaking at about 200 during 50-100 ps. As for CO₂, the number also gradually increased to about 230. Heavier products such as TPA radicals first increased but then gradually decreased during the one ns simulation. Moreover, since no C₆H₅ was detected, the reformation of long-chain species can reasonably explain the consumption of TPA. Overall, during the reaction, the long-chain breaking process first released C₂H₄ and TPA, followed by the production of CO2 associated with the long-chain's reforming process. As will be discussed in the next section, pyrolysis at a temperature range of 1100 to 1600 K was further simulated to understand the impact of temperature on the product distribution and better reveal the reaction pyrolysis mechanism.

Effects of Pyrolysis Temperature. Figure 5 shows the effect of the temperature on the time evolution of species observed in PET pyrolysis. For clarity, only two groups $(C_{2000-100})$ and C_{99-21} were considered to represent all long

and medium chains, respectively. Following the order of the chain lengths of the observed species, the long chain, medium chain, and C_{20-9} groups were first studied. As shown in Figure 5a-c, one narrow peak for the breaking process and one broad peak for the reforming reaction were observed at different temperatures. Moreover, both peaks became narrower as the temperature increased, indicating that higher temperatures can accelerate, as expected, both the cracking of the initial PET long chain and the reforming of shorter-chain species. By contrast, their behavior over temperature is distinctly different for the main gas species with a carbon number under 20. Figure 5d shows that C₈₋₅ (mainly TPA) was generated and then consumed. Unlike those longer-chain groups, no reformation events were observed, leading to a single peak with a maximum yield observed during pyrolysis. It should be noted that at a relatively low temperature of, e.g., 1100 K, no peak was observed since the reaction was too slow. As for C_{4-2} and C_{1-0} , there was no further consumption after these species were generated. From Figure 5e, C_{4-2} (mainly C_2H_4) moieties in all monomers were released rapidly, and it is observed that the release of C₂H₄ was faster under higher temperatures but

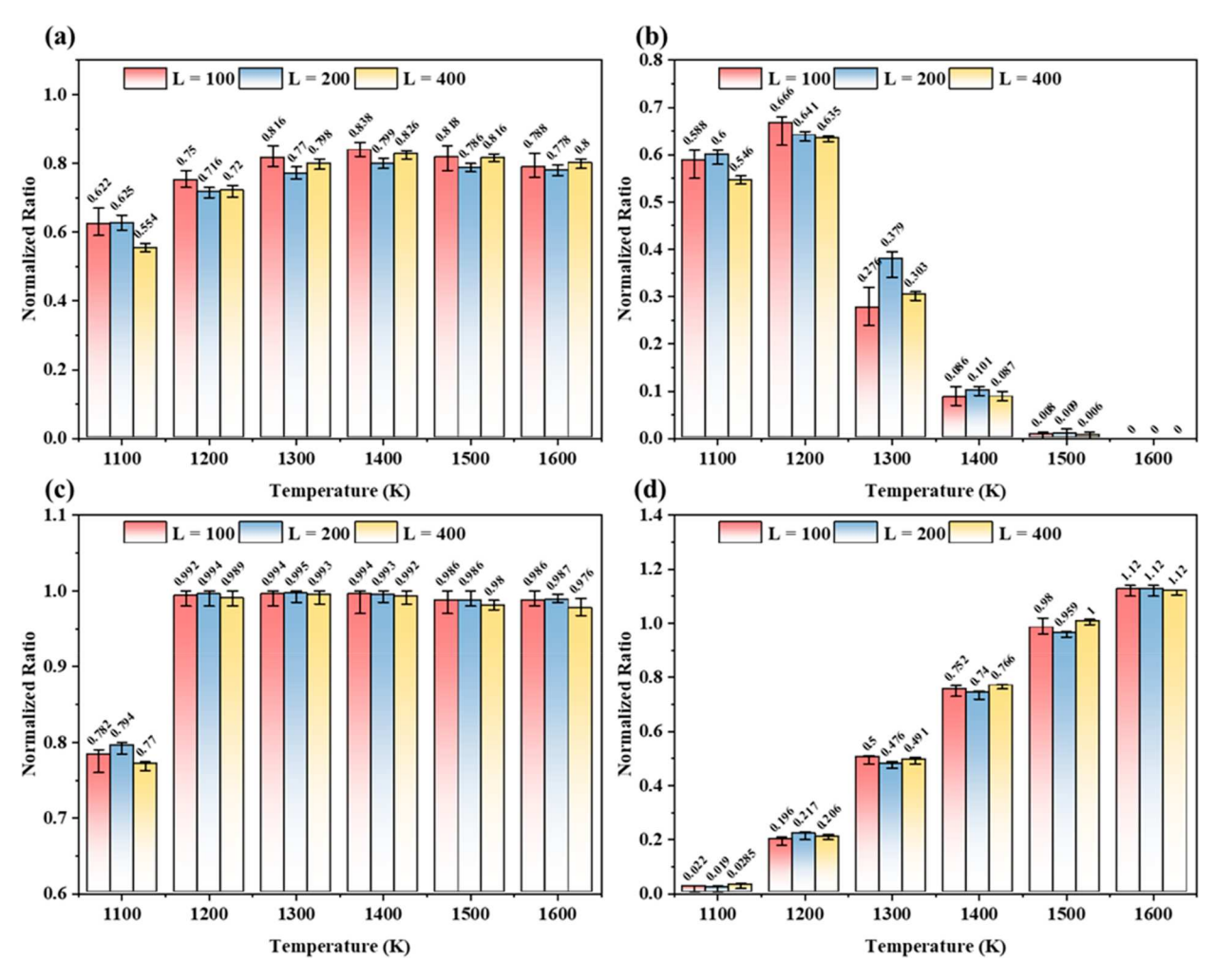


Figure 7. Effect of polymer length L (L = 100, 200, and 400) on the evolution of main species with averaged values of normalized ratio (i.e., normalized ratio = number of species N/polymer length L) from five MD runs with different random seeds: (a) The maximum normalized ratio of TPA radicals observed during one ns simulations and the normalized ratio of (b) TPA radicals, (c) C_2H_4 , and (d) CO_2 observed at the end of simulations at temperatures ranging from 1100 to 1600 K.

the maximum value was around 200 and not affected by temperatures. Similar to C_{4-2} , C_{1-0} (mainly CO_2) species were also not consumed. Figure 5f shows that the accelerated reaction will result in a higher number of C_{1-0} (mainly CO_2) during the one ns simulation since C_{1-0} has not reached equilibrium.

Aside from the above discussion on the species evolution, the total number of reactions observed during PET pyrolysis was also quantified to understand the influence of temperatures on reaction rates and validate the existence of long-chain reforming. Reactions related to long-chain species were first analyzed to determine the length range for the chain reforming reaction. From comparing the number of consumption and generation reaction events at different temperatures, Figure 6a,b shows that the number of both events for $A(C_{2000-1000})$ and $B(C_{999-500})$ was higher at lower temperatures. As the temperature increases, the long-chain breaking becomes irreversible, leading to fewer reactions that involve long-chain species. Since there are reactions for shorter chains that reform into a longer chain, the number of reactions for $C(C_{499-100})$, $D(C_{99-50})$, and $E(C_{49-21})$ first decreased with temperature because the cracking reaction was faster and then increased with temperature due to long chain reforming reaction (Figure 6c-e). If the temperature is too high, the cracking will be aggressive, such as in the reaction of $C_{28} \rightarrow 3C_8 + 2C_2$ (E \rightarrow G + H). This leads to the results shown in Figure 6f that the number of species of $F(C_{20-9})$ will be lower. For gas species such as $G(C_{8-5})$, $H(C_{4-2})$, and $I(C_{1-0})$ (Figure 6g-i), the number of generating and consuming reactions increased with temperatures but at different rates; this results in the different numbers of species accumulated at the end of the simulation. For C₈₋₅ at high temperatures, the difference in the number was marginal, resulting in a low C₈₋₅ yield at the end of the simulation. On the other hand, both C_{4-2} and C_{1-0} always had a higher generation rate at high temperatures, which resulted in the accumulation of these species at the end of the simulation. Although both the number of generation and consumption reaction events for C₄₋₂ increased with temperatures, the difference remained similar since the chemical reactions related to C₄₋₂ reached an equilibrium state after a fast accumulation process. That is, a similar final number of C_{4-2} at the end of one ns simulations at temperatures ranging from 1200 to 1600 K was observed. As for C_{1-0} , the number difference between generation and consumption reaction events kept increasing with time, resulting in more C_{1-0} being observed at the end of the simulation. Overall, the results suggest that the reaction rate increases with temperature as would be expected, but more importantly, the species are generated and consumed

pubs.acs.org/JPCA

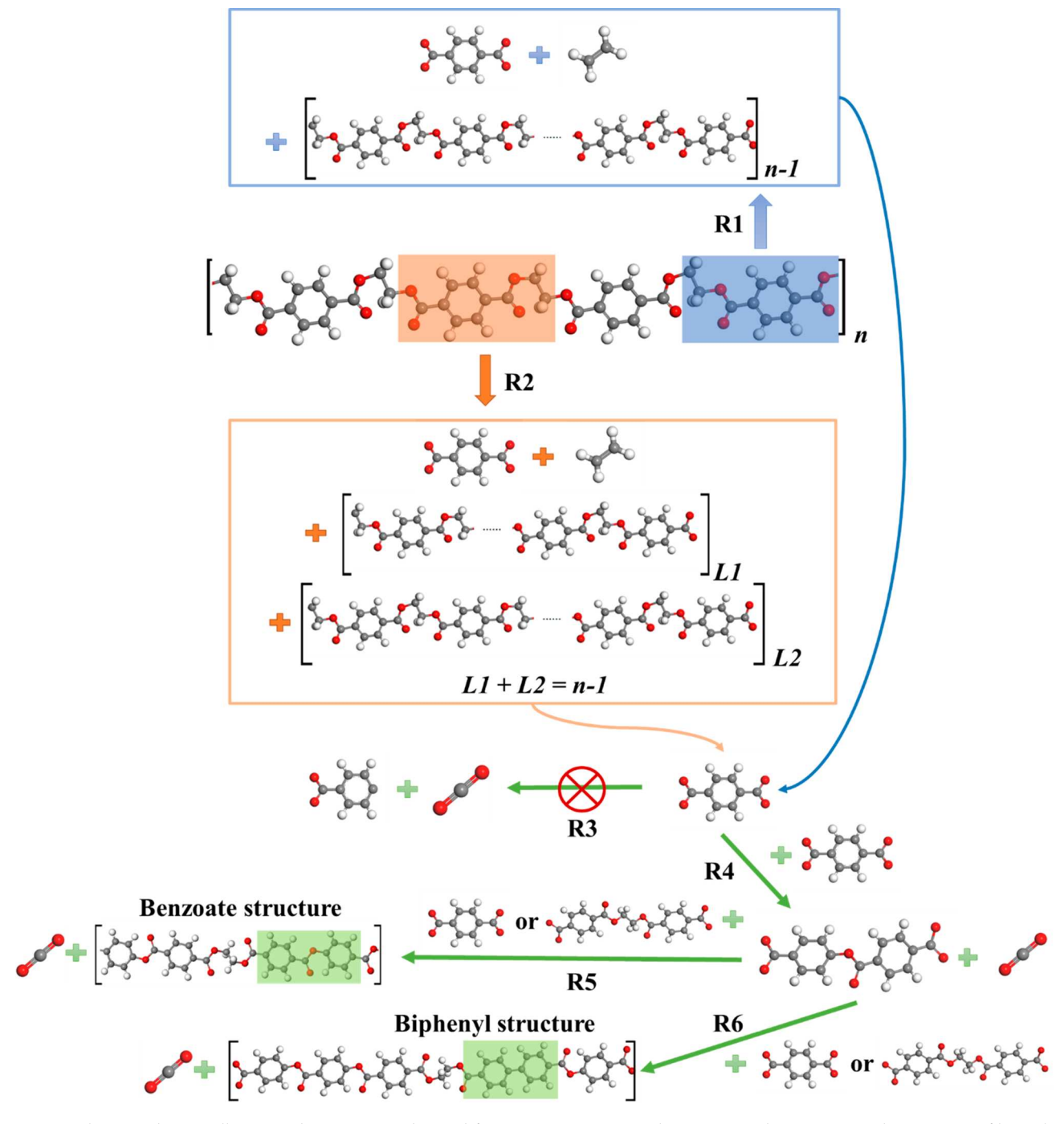


Figure 8. Schematic diagram illustrating key reactions observed from atomistic MD simulations. R1 and R2 represent the reactions of long-chain species breaking from the end or near the middle point, respectively. R3 represents the direct decomposition of TPA, while R4 represents the merging of two TPA molecules. R5 and R6 illustrate the reaction routes of long-chain reformation resulting in benzoate structures or biphenyl structures, respectively. In this figure, *n*, *L*1, and *L*2 refer to the monomer number of species.

simultaneously, while the cracking mechanism for producing gas species is found to be similar (see more details about the change of reaction rate in Figure S3); regardless of the temperature, the long-chain PET cracking produces C_2H_4 and TPA species, while TPA can further fuse into long-chain species and release CO_2 .

Effects of Polymer Length. PET models with different initial chain lengths were simulated to probe the influence of the chain length and the size effect. In order to better present the results, the number of observed molecules is normalized through dividing the observed number by the polymer length

(i.e., number of species N/polymer length L) for the systems, which is termed the normalized ratio. Figure 7a shows the maximum normalized ratio of TPA under varying temperature-length combinations; it is observed that except at 1100 K when the reaction is still in the early stage, the highest ratios were similar for all three lengths from 1200 to 1600 K. Figure 7b also shows the number of TPA observed at the end of the simulations, and for all three different lengths, the normalized ratios of TPA remained similar for different chain lengths within statistical uncertainty. Figure 7c indicates that for 1200-1600 K, the C_2H_4 yield reached maximum values almost

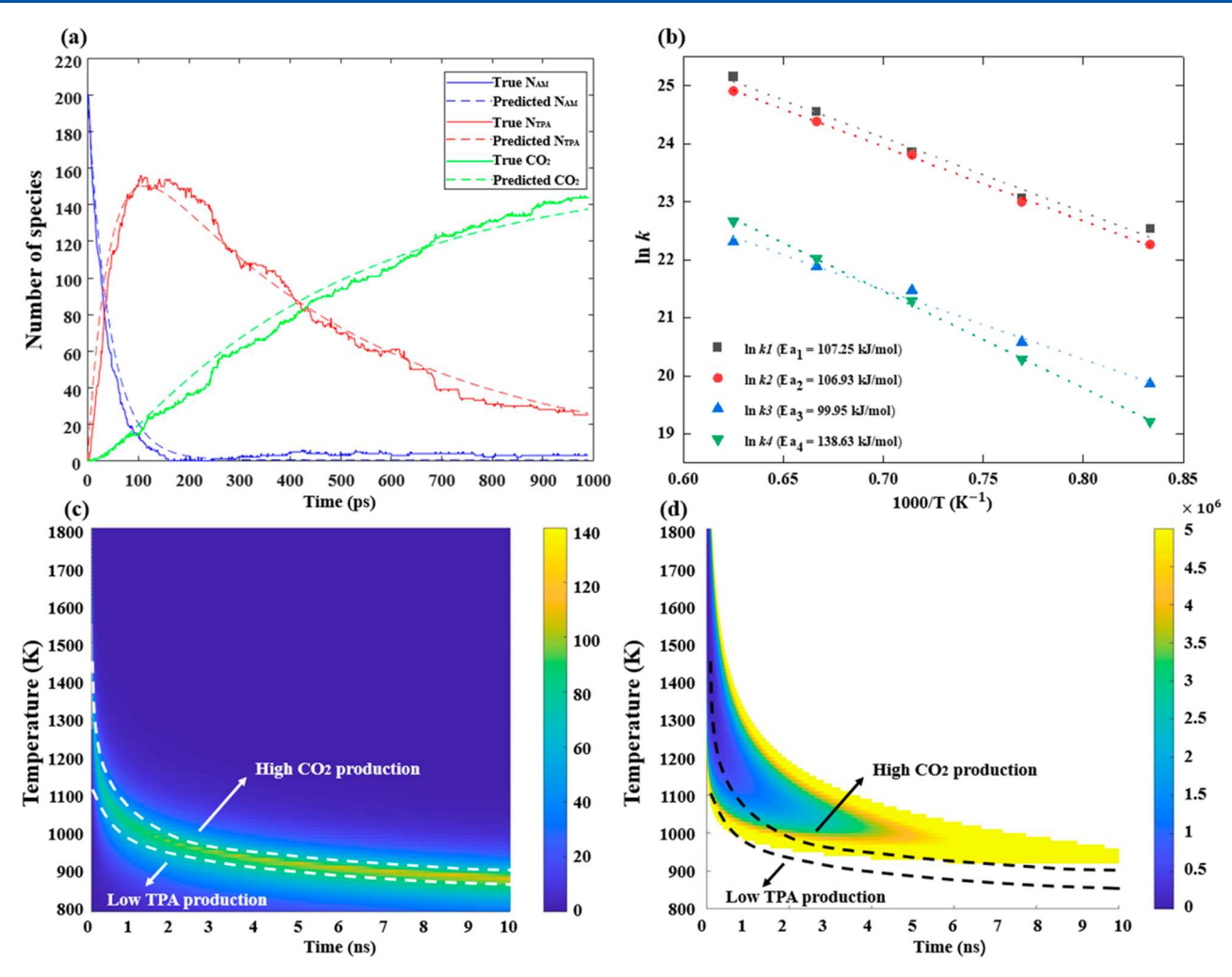


Figure 9. (a) Comparison between the kinetic model and MD data at 1400 K. (b) Activation energies for all kinetic constants calculated by fitting the Arrhenius equation. (c) The TPA/CO_2 ratio and (d) environmental impact factor were determined by using the developed kinetic model. It should be noted that the dashed lines shown in both panels (c) and (d) are identical, and the color is set to white in (d) for values higher than 5×10^6 .

equal to L (i.e., the initial length of the PET molecule) with the normalized ratio equal to 1, while Figure 7d shows that CO_2 production under different temperatures is proportional to the initial chain length as well since the normalized ratio showed similar value for all the chain lengths. Overall, the results suggest that the initial length of the PET polymer did not affect its product types, indicating that the simulation domain adopted is sufficiently large.

Reaction Mechanism. Figure 8 schematically depicts a cracking-reforming mechanism proposed per results discussed thus far for rapid PET pyrolysis. In the initial stage, cracking from the midpoint of the chain (R2) is the primary reaction, which explains the rapid decrease in the chain length. Cleavages at the end of the chains also occur, which is consistent with the smaller slope of the chain length change after the rapid decrease. The breaking process (R1 and R2) will produce C₂H₄ and TPA radicals, while the C₂H₄ will not decompose further. TPA radicals will not directly decompose (R3) either; instead, TPA radicals are involved in a condensation reaction (R4) with the release of CO₂ as a product, followed by forming long chains (also release of CO₂ as a product) with the phenyl benzoate structures (R5) or the biphenyl structure (R6). This mechanism successfully explains the change in chain length and gas production at different

temperatures. Higher temperatures lead to a faster release of TPA and the faster formation of biphenyl structures with greater chain lengths. By contrast, at lower temperatures, more short phenyl benzoate chains are favorably produced, which releases less CO₂ since the growth of the benzoate chain is rather limited. The limited formation of biphenyl structures at lower temperatures also yields less CO₂. This mechanism explains the distribution of the main gas species, especially the formation of CO₂. It also fits with the reversibility of the chain length change observed in the aforementioned rate analysis. Moreover, the mechanism proposed above can be deemed general since the effect of polymer length on the evolution of main species was studied, and the results suggest that the initial length of PET polymer did not affect its product evolution.

Kinetic Modeling. While one could use the information on activation energy with the associated prefactor to predict the overall weight loss of PET pyrolysis at different temperatures, details on specific species are completely missing. Herein, a kinetic model capable of describing the reaction of major species involved in the pyrolysis process (i.e., C₂H₄, TPA, and CO₂) was developed. With the understanding of the mechanism and the reaction route for the main gas species discussed above, a kinetic model comprising a set of differential

equations (i.e., eqs 1-3)) capable of describing the evolution of the main species over time was proposed.

$$\frac{\mathrm{d}N_{\mathrm{AM}}}{\mathrm{d}t} = -k_{\mathrm{I}}N_{\mathrm{AM}} \tag{1}$$

$$\frac{\mathrm{d}N_{\mathrm{TPA}}}{\mathrm{d}t} = k_2 N_{\mathrm{AM}} - k_3 N_{\mathrm{TPA}} \tag{2}$$

$$\frac{\mathrm{d}N_{\mathrm{CO}_2}}{\mathrm{d}t} = -k_4 N_{\mathrm{TPA}} \tag{3}$$

As discussed above, the pyrolysis process of PET can be summarized as breaking of the long chain to produce TPA, and TPA continues the reaction to release CO₂. First, it is noted that the monomers in the long chain act as reactants to release both C₂H₄ and TPA through chain cracking reactions. Since C₂H₄ was not further decomposed, the number of C₂H₄ reflects the number of monomers consumed and can eventually reach a value close to the total number of monomers (i.e., L). Therefore, in this model, we define a term called "active monomer, N_{AM} " which is equivalent to the total number of monomers minus the number of C₂H₄ (i.e., $N_{\rm AM} = N_{\rm PETmonomer} - N_{\rm C2H4}$). The number of active monomers roughly represents the remaining monomers that can still be further reacted to produce TPA. At the beginning of the reaction, the system includes only one long chain containing active monomers with the number of L; namely, the initial condition of the kinetics model is set to be $N_{AM} = L$, $N_{TPA} = 0$, and $N_{\rm CO2}$ = 0. The consumption of active monomers in the kinetic model is described by eq 1, in which the reaction rate of consuming active monomers is proportional to the $N_{\rm AM}$. Second, eq 2 was used for describing the reaction of TPA, which contains reaction constant k_2 representing the formation of TPA from active monomers and reaction constant k_3 representing the merge of TPA into long chains. Since there are also chain cleavage reactions that produce only C2H4 without TPA as side reactions, the rate constant (k_2) is distinct from the active monomer consumption rate constant (k_1) in eq 1. Third, CO₂ is released during the fusion of TPA (R4) and the formation of long chains with benzoate (R5) or biphenyl (R6) structures. From the mechanistic analysis, the growth limitation of benzoate chains and the production of biphenyl structures affect the ratio of CO2 formation to TPA consumption. Since TPA will be consumed for releasing CO2, the rate of carbon dioxide formation is naturally associated with the number of TPA as described by eq 3. Figure 9a shows that the proposed model with the involved parameters optimized closely resembles the results from the MD simulations. Moreover, Figure S4 indicates that the fitting results at temperatures ranging from 1200 to 1600 K are all with good accuracy. Figure 9b further shows the calculated activation energies by fitting to the Arrhenius equation for the parametrized kinetic constants (Table S2). For the release and formation of C₂H₄ and TPA described, respectively, in eqs 1 and 2, it is found that the activation energies are similar. This suggests similar rates for these two processes. The associated kvalues (i.e., k_1 and k_2) at different temperatures are also comparable, which is consistent with the MD observation that C₂H₄ and TPA radicals are almost released simultaneously. On the other hand, a significantly higher activation energy was observed for CO2 release compared to TPA consumption which is consistent with the MD observation that the release of CO₂ is the slower step compared with C₂H₄ and TPA.

Moreover, because of larger pre-exponential factors of k_4 than k_3 , the consumption rate of TPA (k_3) is lower than the formation rate of CO_2 (k_4) at high temperatures. Overall, this again agrees with previous findings of the slow generation of the benzoate chain at lower temperatures and the reduced number of biphenyl structures with a lower production of CO_2 . Overall, the results discussed above demonstrate that the developed model is capable of describing the PET pyrolysis process. We note that the kinetic model may be extended to describe a broader range of species rather than only those dominant species, though the parameter space associated with the model will become much larger.

With the reliable kinetic model and its corresponding rate constants and activation energies, it is possible to access the species distribution under different temperatures (i.e., 800-1800 K) and with a larger time scale. Since among the gas species TPA is a widely used chemical product and a critical reactant for producing PET plastic, while CO_2 is the primary greenhouse gas, it should be reduced. The TPA/ CO_2 molar ratio as a function of the reaction time and temperature was therefore calculated. Besides, an environmental energy impact metric³⁹ (i.e., eqs 4–6)) was incorporated to determine the environmental impact of PET pyrolysis.

$$\varepsilon = \frac{\text{yield}_{\text{TPA}}}{T \times t} \tag{4}$$

$$E = (m_{\text{total}} - m_{\text{TPA}} - m_{\text{C}_2\text{H}_4}) / m_{\text{TPA}}$$
 (5)

$$\xi = E/\varepsilon \tag{6}$$

The energy efficiency coefficient ε , defined in eq 4, is first calculated, where t is the reaction time, T is the reaction temperature, and $yield_{TPA}$ is the yield of the main recyclable monomers. The ε coefficient normalizes the yield of the main monomer produced from the depolymerization process with the required reaction time and temperature. The main monomer in PET pyrolysis is TPA. The lower the temperature and the shorter the reaction time are, the higher the relative value of ε . Besides, to consider the amount of waste produced during the process, the *E* factor, as shown in eq 5 from Sheldon et al., was computed as the mass ratio of waste over TPA. Herein, the mass of waste was considered as the mass of species other than C_2H_4 and TPA. With ε and E, the environmental energy impact ξ , which is defined in eq 6, can be accordingly calculated. It represents the combined effect of the mass input and the energy economy, and the pyrolysis process with a lower ξ is obviously preferred. Figure 9c shows the TPA/CO₂ ratio as a function of the temperature and reaction time. The results show that the TPA/CO2 ratio is smaller in the lower left region, caused by the slow production of TPA at low temperatures. As the temperature rises, the consumption of TPA and the excessive amount of CO2 again lead to low ratios (i.e., the upper right region). It is noted that under higher temperatures, the reaction time for achieving a larger TPA/CO₂ ratio should be shorter; with the consumption of TPA, it reaches zero in the later stage of the reaction since all the TPA radicals are consumed. Figure 9d correspondingly shows the computed environmental impact factor (Figure 9d). The ξ value is high for pyrolysis conducted at lower temperatures due to slow TPA production. At higher temperatures, although ξ is small at the beginning of the reaction, it increases rapidly as the reaction proceeds because TPA is consumed, and the heat input also increases with time.

By comparing the TPA/CO₂ ratio (Figure 9c) and the environmental impact factor (Figure 9d), the area with low environmental impact factor (regions of dark blue color shown in Figure 9d) can exist between the boundary with the ideal product distribution (within the black dashed lines shown in Figure 9d). That is, operating PET pyrolysis at a higher temperature (over 1100 K) with limited reaction time (far away from equilibrium) may be an optimal strategy for reaching a high TPA/CO₂ ratio with a low environmental impact. And in recent experimental study of PET pyrolysis, ⁴¹ this strategy (i.e., fast pyrolysis with a high temperature) is also proven to be effective in reaching a high degree of depolymerization and an improved monomer yield.

CONCLUSIONS

In this work, molecular dynamics (MD) simulations based on reactive force fields (ReaxFF) were performed to study the pyrolysis of PET. The accuracy of adopted ReaxFF was first validated by comparing the density and activation energy with experimental data. A cracking-reforming mechanism was unraveled for PET pyrolysis. At the initial stage, PET longchain cracking started with C-O bond dissociation that occurred preferentially near the middle point of the polymer chain, resulting in fast chain breaking while producing C₂H₄ and TPA radicals. During pyrolysis, the reaction rate for gas products increases with temperature, but C₂H₄ and CO₂ will not undergo further decomposition. However, TPA radicals will undergo a condensation reaction to form long chains with phenyl benzoate structures, which increases the number of long-chain species in the later stage of the reaction at higher temperatures. When the temperature decreases, the growth of phenyl benzoate chains and the formation of biphenyl structures become limited, resulting in less CO₂ production. A kinetic model, comprising a set of differential equations, was also developed to describe observations from atomistic molecular dynamics simulations. The kinetic model identified that a higher temperature (over 1100 K) with limited reaction time would be optimal for a high TPA/CO2 ratio for potentially better circularity and lower environmental impact. Overall, this study successfully bridges atomistic findings of PET pyrolysis and macroscopic reaction modeling, extrapolating the observations made within a few nanoseconds at high temperatures to practical operating conditions. It is anticipated that the approach reported herein can also be applied to study the pyrolysis of other polymer materials or even decomposition reactions assisted by catalysts or solvents.

ASSOCIATED CONTENT

Supporting Information

The Supporting Information is available free of charge at https://pubs.acs.org/doi/10.1021/acs.jpca.3c03717.

Temperatures and chain length of simulated PET systems, kinetic constants fitted from the proposed kinetic model at temperatures ranging from 1200 to 1600 K, comparison between the simulated and reported activation energies and products distribution for PET pyrolysis, snapshots of simulated PET systems at 1600 K, long and midchain species distribution at the beginning stage of PET pyrolysis at 1600 K, reaction rate and reversibility, validation of the proposed kinetic model (PDF)

Simulation input files for the ReaxFF simulations of PET systems (ZIP)

AUTHOR INFORMATION

Corresponding Authors

Li-Chiang Lin — William G. Lowrie Department of Chemical and Biomolecular Engineering, The Ohio State University, Columbus, Ohio 43210, United States; Department of Chemical Engineering, National Taiwan University, Taipei 10617, Taiwan; Occid.org/0000-0002-2821-9501; Email: lclin@ntu.edu.tw

Bhavik R. Bakshi — William G. Lowrie Department of Chemical and Biomolecular Engineering, The Ohio State University, Columbus, Ohio 43210, United States; orcid.org/0000-0002-6604-8408; Email: bakshi.2@osu.edu

Authors

Shuangxiu Max Ma — William G. Lowrie Department of Chemical and Biomolecular Engineering, The Ohio State University, Columbus, Ohio 43210, United States

Changlong Zou — William G. Lowrie Department of Chemical and Biomolecular Engineering, The Ohio State University, Columbus, Ohio 43210, United States; orcid.org/0000-0002-1390-5859

Ting-Yeh Chen – William G. Lowrie Department of Chemical and Biomolecular Engineering, The Ohio State University, Columbus, Ohio 43210, United States

Joel A. Paulson – William G. Lowrie Department of Chemical and Biomolecular Engineering, The Ohio State University, Columbus, Ohio 43210, United States; orcid.org/0000-0002-1518-7985

Complete contact information is available at: https://pubs.acs.org/10.1021/acs.jpca.3c03717

Notes

The authors declare no competing financial interest.

ACKNOWLEDGMENTS

S.X.M. acknowledges the financial support from the National Science Foundation through Grant EFMA2029397. L.C.L. acknowledges the support from the Yushan Young Program of the Ministry of Education in Taiwan (NTU-110VV009), the National Science and Technology Council in Taiwan (110-2222-E-002-011-MY3), and the Excellence in Key Advantages Program at National Taiwan University (NTU-CC-112L893106). We also gratefully acknowledge computational resources from the Ohio Supercomputer Center (OSC).

REFERENCES

- (1) Park, C.-H.; Jeon, H.-S.; Yu, H.-S.; Han, O.-H.; Park, J.-K. Application of electro-static separation to the recycling of plastic wastes: separation of PVC, PET, and ABS. *Environ. Sci. Technol.* **2008**, 42, 249–255.
- (2) Dodbiba, G.; Takahashi, K.; Sadaki, J.; Fujita, T. The recycling of plastic wastes from discarded TV sets: comparing energy recovery with mechanical recycling in the context of life cycle assessment. *J. Cleaner Prod.* **2008**, *16*, 458–470.
- (3) Sadat-Shojai, M.; Bakhshandeh, G.-R. Recycling of PVC wastes. *Polym. Degrad. Stab.* **2011**, *96*, 404–415.
- (4) Li, Č.-T.; Lee, W.-J.; Mi, H.-H.; Su, C.-C. PAH emission from the incineration of waste oily sludge and PE plastic mixtures. *Sci. Total Environ.* **1995**, *170*, 171–183.

- (5) Wong, S.; Ngadi, N.; Abdullah, T. A. T.; Inuwa, I. M. Current state and future prospects of plastic waste as source of fuel: A review. *Renewable Sustainable Energy Rev.* **2015**, *50*, 1167–1180.
- (6) Kunwar, B.; Cheng, H.; Chandrashekaran, S. R.; Sharma, B. K. Plastics to fuel: a review. *Renewable Sustainable Energy Rev.* **2016**, 54, 421–428.
- (7) Luo, W.; Hu, Q.; Fan, Z.-y.; Wan, J.; He, Q.; Huang, S.-x.; Zhou, N.; Song, M.; Zhang, J.-c.; Zhou, Z. The effect of different particle sizes and HCl-modified kaolin on catalytic pyrolysis characteristics of reworked polypropylene plastics. *Energy* **2020**, *213*, No. 119080.
- (8) Kiran Ciliz, N.; Ekinci, E.; Snape, C. E. Pyrolysis of virgin and waste polypropylene and its mixtures with waste polyethylene and polystyrene. *Waste Manage.* **2004**, *24*, 173–181.
- (9) Brophy, J.; Hardman, S. Low temperature pyrolysis for feedstock preparation. *Recycl. Recovery Plast.* **1996**, 422–433.
- (10) Pinto, F.; Costa, P.; Gulyurtlu, I.; Cabrita, I. Pyrolysis of plastic wastes: 2. Effect of catalyst on product yield. *J. Anal. Appl. Pyrolysis* **1999**, *51*, 57–71.
- (11) Pinto, F.; Costa, P.; Gulyurtlu, I.; Cabrita, I. Pyrolysis of plastic wastes. 1. Effect of plastic waste composition on product yield. *J. Anal. Appl. Pyrolysis* **1999**, *51*, 39–55.
- (12) Dimitrov, N.; Krehula, L. K.; Sirŏci'c, A. P.; Hrnjak-Murgi'c, Z. Analysis of recycled PET bottles products by pyrolysis-gas chromatography. *Polym. Degrad. Stab.* **2013**, *98*, 972–979.
- (13) Mart'in-Gull'on, I.; Esperanza, M.; Font, R. Kinetic model for the pyrolysis and combustion of poly(ethylene terephthalate) (PET). *J. Anal. Appl. Pyrolysis* **2001**, *58-59*, 635–650.
- (14) Zhang, H.; Zhou, X.-L.; Shao, L.-M.; Lü, F.; He, P.-J. Upcycling of PET waste into methane-rich gas and hierarchical porous carbon for high-performance supercapacitor by autogenic pressure pyrolysis and activation. *Sci. Total Environ.* **2021**, 772, No. 145309.
- (15) Suriapparao, D. V.; Kumar, D. A.; Vinu, R. Microwave copyrolysis of PET bottle waste and rice husk: effect of plastic waste loading on product formation. *Sustain. Energy Technol. Assess.* **2022**, 49, No. 101781.
- (16) Adnan; Shah, J.; Jan, M. R. Effect of polyethylene terephthalate on the catalytic pyrolysis of polystyrene: Investigation of the liquid products. *J. Taiwan Inst. Chem. Eng.* **2015**, *51*, 96–102.
- (17) Çepeliŏgullar, Ö; Pütün, A. E. Utilization of two different types of plastic wastes from daily and industrial life. *Journal of Selcuk University Natural and Applied Science* **2013**, *2*, 694–706.
- (18) Grause, G.; Handa, T.; Kameda, T.; Mizoguchi, T.; Yoshioka, T. Effect of temperature management on the hydrolytic degradation of PET in a calcium oxide filled tube reactor. *Chem. Eng. J.* **2011**, *166*, 523–528.
- (19) Du, S.; Valla, J. A.; Parnas, R. S.; Bollas, G. M. Conversion of polyethylene terephtha- late based waste carpet to benzene-rich oils through thermal, catalytic, and catalytic steam pyrolysis. *ACS Sustainable Chem. Eng.* **2016**, *4*, 2852–2860.
- (20) Wang, K.; Zhang, J.; Shanks, B. H.; Brown, R. C. Catalytic conversion of carbohydrate- derived oxygenates over HZSM-5 in a tandem micro-reactor system. *Green Chem.* **2015**, *17*, 557–564.
- (21) Masuda, T.; Kushino, T.; Matsuda, T.; Mukai, S. R.; Hashimoto, K.; Yoshida, S.-i. Chemical recycling of mixture of waste plastics using a new reactor system with stirred heat medium particles in steam atmosphere. *Chem. Eng. J.* 2001, 82, 173–181.
- (22) Kumagai, S.; Yamasaki, R.; Kameda, T.; Saito, Y.; Watanabe, A.; Watanabe, C.; Tera- mae, N.; Yoshioka, T. Aromatic hydrocarbon selectivity as a function of CaO basicity and aging during CaO-catalyzed PET pyrolysis using tandem μ -reactor-GC/MS. *Chem. Eng. J.* **2018**, 332, 169–173.
- (23) Obuchi, E.; Suyama, M.; Nakano, K. Decomposition of mixed plastics consisting of polypropylene and polyethylene terephthalate into oils over titania/silica catalysts. *J. Mater. Cycles Waste Manage.* **2001**, *3*, 88–92.
- (24) Huang, J.; Meng, H.; Luo, X.; Mu, X.; Xu, W.; Jin, L.; Lai, B. Insights into the ther- mal degradation mechanisms of polyethylene terephthalate dimer using DFT method. *Chemosphere* **2022**, 291, No. 133112.

- (25) Cabianca, L.; Bassani, A.; Amaral, A. F.; Rossi, F.; Bozzano, G.; Ranzi, E.; Telen, D.; Logist, F.; Van Impe, J.; Manenti, F. GASDS: a kinetic-based package for biomass and coal gasification. *Chem. Eng. Trans.* **2016**, *50*, 247–252.
- (26) Van Duin, A. C.; Dasgupta, S.; Lorant, F.; Goddard, W. A. ReaxFF: a reactive force field for hydrocarbons. *J. Phys. Chem. A* **2001**, 105, 9396–9409.
- (27) Chenoweth, K.; Van Duin, A. C.; Goddard, W. A. ReaxFF reactive force field for molecular dynamics simulations of hydrocarbon oxidation. *J. Phys. Chem. A* **2008**, *112*, 1040–1053.
- (28) Chen, Z.; Sun, W.; Zhao, L. High-temperature and high-pressure pyrolysis of hexade- cane: molecular dynamics simulation based on reactive force field (ReaxFF). *J. Phys. Chem. A* **2017**, *121*, 2069–2078.
- (29) Chen, Z.; Zhao, P.; Zhao, L.; Sun, W. Molecular simulation of the catalytic cracking of hexadecane on ZSM-5 catalysts based on reactive force field (ReaxFF). *Energy Fuels* **2017**, *31*, 10515–10524.
- (30) Zeng, J.; Cao, L.; Xu, M.; Zhu, T.; Zhang, J. Z. Complex reaction processes in combus- tion unraveled by neural network-based molecular dynamics simulation. *Nat. Commun.* **2020**, *11*, 5713.
- (31) Chen, Z.; Sun, W.; Zhao, L. Initial mechanism and kinetics of diesel incomplete com- bustion: ReaxFF molecular dynamics based on a multi-component fuel model. *J. Phys. Chem. C* **2019**, *123*, 8512–8521.
- (32) Hong, D.; Li, P.; Si, T.; Guo, X. ReaxFF simulations of the synergistic effect mech- anisms during co-pyrolysis of coal and polyethylene/polystyrene. *Energy* **2021**, *218*, No. 119553.
- (33) Jewett, A. I.; Stelter, D.; Lambert, J.; Saladi, S. M.; Roscioni, O. M.; Ricci, M.; Autin, L.; Maritan, M.; Bashusqeh, S. M.; Keyes, T.; et al. Moltemplate: A tool for coarse-grained modeling of complex biological matter and soft condensed matter physics. *J. Mol. Biol.* **2021**, 433, No. 166841.
- (34) Wang, Q.; Keffer, D. J.; Nicholson, D. M.; Thomas, J. B. Coarse-grained molecular dynamics simulation of polyethylene terephthalate (PET). *Macromolecules* **2010**, 43, 10722–10734.
- (35) Wang, Y. H.; Wang, W. H.; Zhang, Z.; Xu, L.; Li, P. Study of the glass transition temperature and the mechanical properties of PET/modified silica nanocomposite by molecular dynamics simulation. *Eur. Polym. J.* **2016**, *75*, 36–45.
- (36) Thompson, A. P.; Aktulga, H. M.; Berger, R.; Bolintineanu, D. S.; Brown, W. M.; Crozier, P. S.; Plimpton, S. J.; et al. LAMMPS-a flexible simulation tool for particle-based materials modeling at the atomic, meso, and continuum scales. *Comput. Phys. Commun.* **2022**, 271, No. 108171.
- (37) Zhang, J.; Wang, J.; Li, Z.; Zhu, J.; Lu, B. Molecular Dynamics Simulation and Gas Generation Tracking of Pyrolysis of Bituminous Coal. ACS omega 2022, 7 (13), 11190–11199.
- (38) Wei, X.; Yu, J.; Du, J.; Sun, L. New insights into the pyrolysis behavior of polycarbonates: a study based on DFT and ReaxFF-MD simulation under nonisothermal and isothermal conditions. *Energy Fuels* **2021**, 35 (6), 5026–5038.
- (39) Arias, J. J. R.; Thielemans, W. Instantaneous hydrolysis of PET bottles: An efficient pathway for the chemical recycling of condensation polymers. *Green Chem.* **2021**, 23, 9945–9956.
- (40) Sheldon, R. A. The E factor 25 years on: the rise of green chemistry and sustainability. *Green Chem.* **2017**, *19*, 18–43.
- (41) Dong, Q.; Lele, A. D.; Zhao, X.; Li, S.; Cheng, S.; Wang, Y.; Cui, M.; Guo, M.; Brozena, A. H.; Lin, Y.; et al. Depolymerization of plastics by means of electrified spatiotemporal heating. *Nature* **2023**, 616 (7957), 488–494.